18TH WORLD CONFERENCE ON EARTHQUAKE ENGINEERING
WCEE2024
MILAN

MILAN, ITALY
30TH JUNE - 5TH JULY 2024

www.wcee2024.it

RISK-BASED SEISMIC PERFORMANCE ASSESSMENT OF STEEL BUILDINGS WITH SELF-CENTERING FRICTION DEVICES

F. Shi[1], S. Cao[2] and O.E. Ozbulut[3]

[1] School of Physics and Materials Science, Guangzhou University, Guangzhou, China, shifei@gzhu.edu.cn

[2] School of Civil Engineering, Guangzhou University, Guangzhou, China, cao@gzhu.edu.cn

[3] Department of Civil and Environmental Engineering, University of Virginia, Charlottesville, VA, USA, ozbulut@virginia.edu

Abstract: *This study explores comparative seismic performance of a shape memory alloy (SMA)-only device, a hybrid self-centering device, and a friction damper. SMA-based hybrid device considered in this study, named as superelastic friction dampers (SFDs), has been recently proposed and experimentally characterized. A brief description of the device and its mechanical response is presented first. Then, an 8-story archetype steel frame building is designed with each seismic protection device (SMA-only, hybrid self-centering, and friction only) and modeled. To enable comparative performance assessment, each device is designed to have similar initial stiffness and the same maximum force at design displacement. Nonlinear time history analyses are conducted employing a collection of 44 ground motion records. The results are evaluated to compare performance of each frame design at design-basis and maximum considered earthquake hazard levels. Next, a risk-based seismic hazard demand analysis framework that involves comprehensive incremental dynamic analyses is employed for further discussing and comparing the performance of each system. Results indicate that SFDs provides a well-balanced combination of energy dissipation capability and self-centering competence, leading to structures that exhibit minimal transient and residual responses.*

1 Introduction

The increasing transformation of urban landscapes and the persistent challenge of potential seismic hazards continuously test our engineering expertise, underscoring the crucial importance of designing earthquake-resilient buildings. Traditional seismic force-resisting mechanisms such as moment frames, braced frames, and shear walls allow targeted structural elements to withstand controlled damage, ensuring ductility. However, this often results in residual deformations, commonly referred to as “residual drift”. Effective mitigation of residual drift is essential not only for preserving the structural integrity of buildings but also for facilitating post-earthquake recovery (FEMA P58 2012). Consequently, advanced seismic design approaches and seismic protection technologies play a vital role in enhancing the seismic resilience of buildings.

The incorporation of self-centering seismic control devices in structural designs presents a transformative approach to address limitations in the current design paradigm while ensuring sustained functionality in the aftermath of an earthquake event (Zhong & Christopoulos. 2022). These innovative devices not only effectively dissipate energy but also possess the remarkable ability to recenter themselves. By introducing a restoring force either independently or in conjunction with energy dissipation, these devices exhibit a distinct flag-shaped response that enhances their performance. This implies a significant advancement in seismic resilience, as these self-centering devices provide enhanced structural protection and aid in the rapid recovery of buildings following seismic events.

Achieving self-centering capability in seismic control devices can be realized through various mechanisms. These mechanisms include the utilization of post-tensioning elements, disc springs, and shape memory alloys

(Fang et al. 2023). Post-tensioning elements are commonly integrated into traditional energy dissipation systems, such as viscous dampers or friction dampers, to create self-centering dampers (Erochko et al. 2015; Xiao et al. 2022). While this technique offers cost-effective self-centering behavior, it does have certain limitations. These include the complexity and cost associated with prestressing and anchoring tendons, limitations in deformability due to the small elastic strain of pre-tensioned tendons, and the susceptibility of pre-tensioned tendons to creep and relaxation. Another approach for achieving self-centering seismic control devices involves the use of friction springs, also known as ring springs (Xu et al. 2016). These components consist of alternating outer and inner rings with tapered mating surfaces, facilitating energy dissipation through the friction generated between the rings. Alternatively, self-centering devices have been developed utilizing superelastic shape memory alloys (SMAs). SMAs exhibit the remarkable ability to regain their original shape after deformation and subsequent load removal, providing inherent self-centering capability (Ozbulut et al. 2011). Additionally, these alloys offer energy dissipation due to their characteristic hysteresis loop in mechanical behavior. This unique combination of attributes has sparked significant interest in the advancement of seismic protection technologies centered around SMAs.

While certain seismic control devices based on shape memory alloys (SMAs) hinge entirely on the energy dissipation potential of SMAs (Shi et al. 2022), a more recent trend involves blending SMAs with alternative energy dissipation mechanisms to create hybrid devices (Shi et al. 2023; Ping et al. 2022). Initial research efforts on such hybrid devices have concentrated on fabricating and empirically characterizing individual devices, alongside evaluating their seismic effectiveness. However, there are limited studies that comprehensively assess and compare the performance of SMA-only self-centering devices, hybrid self-centering devices, and conventional seismic energy dissipation counterparts.

This study aims to address and evaluate the comparative performance of three different seismic control devices: an SMA-only device, a hybrid self-centering device, and a friction damper. The hybrid device considered in this study, called superelastic friction damper (SFD), combines SMAs with friction dampers and has been recently proposed and experimentally characterized (Asfaw et al. 2022). First, a description of the device and its mechanical response is provided. Then, an 8-story prototype steel frame building is designed to incorporate each of the three seismic protection devices (SMA-only, hybrid self-centering, and friction). Next, nonlinear time history analyses are conducted using a suite of 44 ground motion records. The resulting data is subjected to a comprehensive risk-based seismic hazard demand analysis, providing a framework for a detailed discussion on the comparative effectiveness of each system.

2 Description of Superelastic Friction Damper

Figure 1(a) presents the configuration and working mechanism of the Superelastic Friction Damper (SFD). This damper comprises several key components, including SMA cables, inner and outer steel members, friction pads, slotted end plates, and connection plates. The outer member is constructed from a pair of steel channels, featuring friction pads affixed to the exterior face of the web. The inner member consists of I-shaped steel, with the web serving as a sliding interface for the friction pads. An important aspect in achieving enduring, reliable sliding behavior is the careful selection of the friction interface material. In this study friction pads crafted from metal-free brake and clutch lining, often referred to as non-metallic melded strips are used.

In the case of the damper being subjected to axial tension loading, it is important to consider that no relative movement occurs between the inner and outer members when the applied load (F) is below the static friction force. In this scenario, the axial deformation of the SFD is primarily attributed to the elastic deformation of its members. However, when the tension load surpasses the slip load, the inner member pulls the right end plate, and they move together, while the left end plate remains stationary due to its constraint by the outer member. Consequently, the separation of the two end plates leads to the elongation of the shape memory alloy (SMA) cables. Conversely, when the damper is subjected to compression loading, the opposite conditions occur. In this case, the left end plate moves towards the left as it is pushed by the inner member, while the right end plate remains fixed due to the constraint imposed by the outer member. Thus, both tension and compression loads result in the movement of the end plates, causing elongation in the SMA cables.

Figure 1(b) shows the experimental setup for the SFD specimen. Cyclic loading tests have been conducted to characterize the hysteretic behavior of the SFD. The SFD specimen is connected to an MTS 244 hydraulic actuator, which allows a maximum force of 98 kN and a maximum velocity of 381 mm/sec. The response of the damper at frequencies ranging from 0.02 Hz to 1 Hz is characterized at a displacement amplitude of 20

mm. Figure 1(c) shows the force-displacement response of the SFD under different loading frequencies on the same plot. It can be observed that the behaviour of the damper in the two loading directions look symmetrical. In general, the damper displayed a completely stable, repeatable, and reliable behaviour with insignificant dependence on the frequency for the range considered in this study.

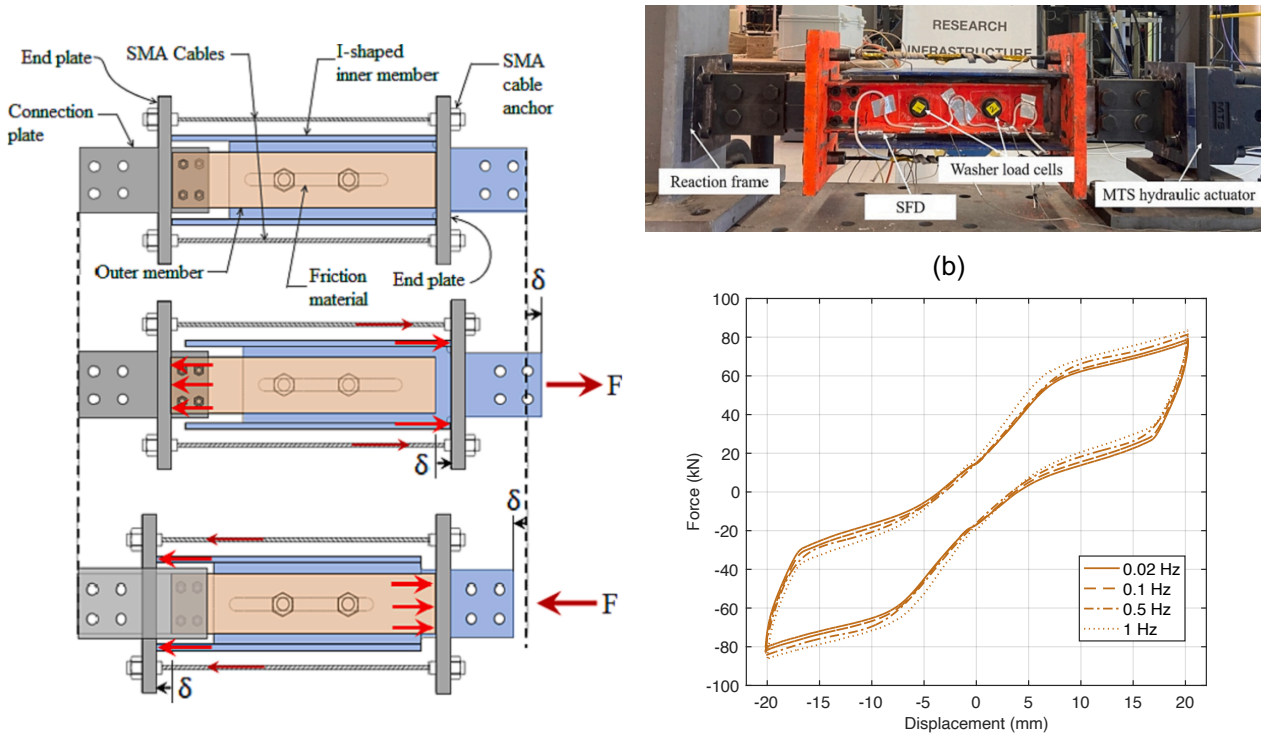

Figure 1. (a) Working mechanism, (b) experimental setup, and (c) hysteretic response at various loading frequencies for the SFD (Asfaw et al., 2022).

3 Numerical modeling

An 8-story office building, classified as a Risk Category II structure and situated in a Class D soil condition (stiff soil), has been chosen as the subject for numerical investigations. This office building is designed with a dual-system steel frame, incorporating both a lateral force-resisting frame and a gravity frame.The floor framing layout and the elevation of the specific east-west orientation of this prototype building are depicted in Figure 2. The selected frame is a symmetrical three-span special moment frame (SMF) positioned along the perimeter of the building. The fundamental period of the chosen steel moment-resisting frame is calculated at 3.81 seconds. More comprehensive information regarding the prototype building can be found in Harris and Speicher (2015).

Numerical modeling of the building is developed in OpenSees. The beam and column components are represented by a concentrated plastic model consisting of elastic beam-column element with rotational springs at both ends to represent plastic hinges. The mechanical behavior of plastic hinges is characterized by using the modified Ibarra–Medina–Krawinkler (IMK) deterioration model for the beams and columns (Ibarra et al. 2005). The shear distortion behavior of the panel zone is modeled following the suggestion of Gupta and Krawinkler and is represented using a trilinear hysteretic model without cyclic degradation considerations (Gupta and Krawinkler 1999). Furthermore, the numerical model accounted for the P-delta effect caused by the interior gravity loads by incorporating an additional leaning column. A Rayleigh damping of 3% is assigned to the steel frame building for numerical modeling.

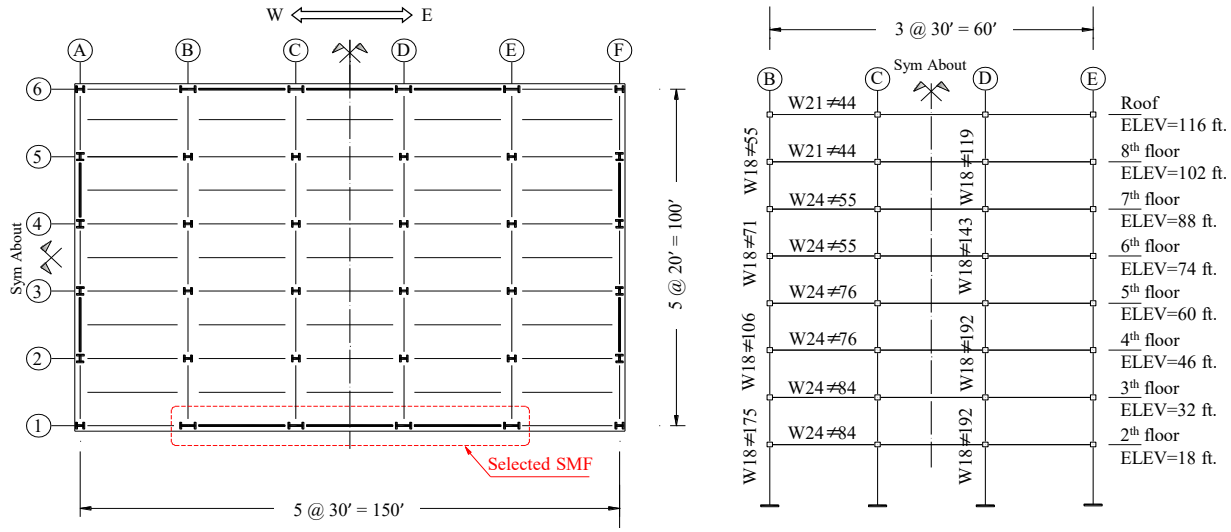

(a) (b)

Figure 2. (a) Plan view, and (b) elevation of the archetype building

The mechanical behavior of the SFD, which comprises both shape memory alloy (SMA) cables and friction components operating in parallel, is simulated using a combination of two distinct mechanical models: Steel02 and self-centering. To assess the suitability of these mechanical models for different dampers, Figure 3 presents a comparative study of the mechanical behavior by comparing experimental results with numerical modeling for various dampers. The loading frequency has minimal influence on the response of the proposed device, thus experimental responses obtained at a dynamic loading rate of 0.5 Hz are utilized to model each component. The simulated hysteretic curves closely match the experimental results, demonstrating that the mechanical models employed in this study accurately capture the hysteretic behavior of various dampers. Furthermore, the SFD can be effectively represented through the parallel combination of the Steel02 and self-centering materials.

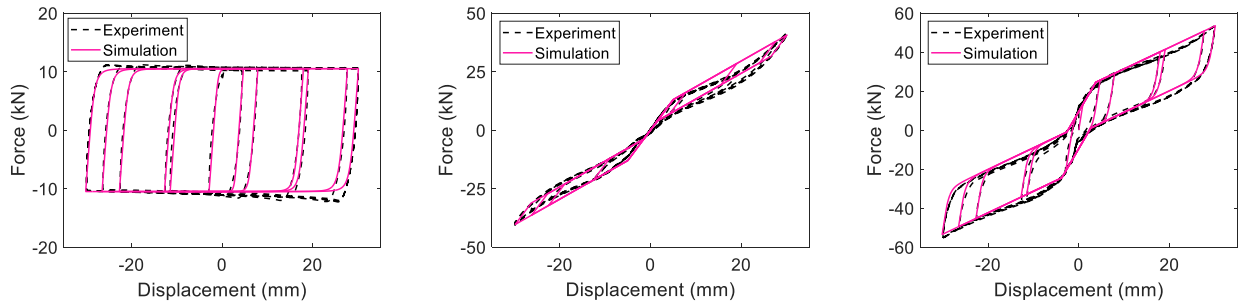

(a) (b) (c)

Figure 3. Comparison of hysteretic behavior between experimental result and numerical simulation for (a) friction damper, (b) SMA cables only, and (c) SFD

In this section, the seismic performance of steel frames equipped with SMA, SFD, and FD systems is compared and evaluated through the design of three case-study frames. The original special moment-resisting frame (SMRF) is modified by converting the two side spans into hinged frames with chevron braced damping systems, as depicted in Figure 4. The beams are connected to the columns through pinned connections with negligible rotational stiffness. The three case-study frames are identified as the FD frame, SFD frame, and SMA frame, respectively, reflecting the different damper configurations employed. To ensure a fair and consistent assessment of the steel frames with various damping systems, the three dampers are designed to possess similar initial stiffness and the same maximum force at the designated displacement, as illustrated in Figure 6 (b). The design displacement, in accordance with ASCE 7-16, is 1.2 times the deformation generated by the dampers under Maximum Considered Earthquake (MCE) hazard level seismic excitation. Table 1 provides a summary of the mechanical model parameters utilized for the different dampers at various floors in each of the three case-study frames. The fundamental periods of the FD frame, SFD frame, and SMA frame are 1.30s, 1.46s, and 1.45s, respectively.

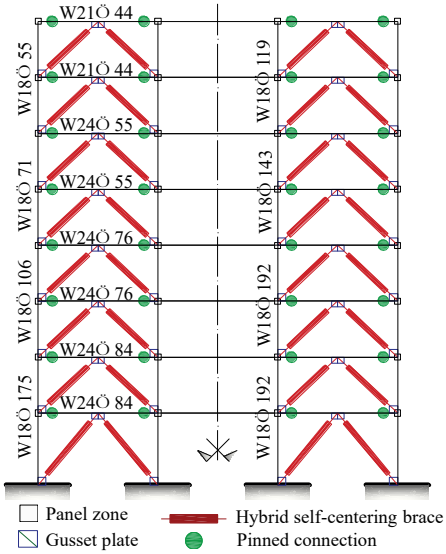

Figure 4. Configuration of steel frame building with damping systems

Table 1. Parameters of various mechanical models for three case-study frames

Case-study building	Story	Self-centering material				Steel02 material		
		Initial stiffness (kN/mm)	Post- activation stiffness (kN/mm)	Forward activation Force (kN)	Ratio of forward to reverse activation force	Yield strength (kN)	Initial stiffness (kN/mm)	Strain-hardening ratio
FD Frame	1-2			-		600	300	0
	3-4					550	275	0
	5-6					500	250	0
	7-8					450	225	0
SFD Frame	1-2	10	1.80	200	0.1	180	180	0
	3-4	10	1.63	200	0.1	160	160	0
	5-6	9	1.50	180	0.1	140	140	0
	7-8	8	1.43	160	0.1	120	120	0
SMA Frame	1-2	200	1.481	400	0.4	-		
	3-4	175	1.481	350	0.4			
	5-6	150	1.481	300	0.4			
	7-8	125	1.481	250	0.4			

4 Risk-based seismic performance assessment

To evaluate the seismic performance of the steel frame equipped with Self-Centering Friction Dampers (SFDs), a total of 44 far-field ground motion records are selected for nonlinear dynamic analyses. These records are chosen from the PEER NGA database and recommended by FEMA P695 for assessing the seismic performance of structures. The nonlinear time history analyses of the three case-study frames are conducted using OpenSees. A 10-second free vibration time is included after each ground motion record to obtain a relatively stable residual deformation response.

The seismic demand hazard analysis provides the mean annual frequency, $\lambda_{EDP}(d)$, that the engineering demand parameter (EDP) exceeds any specified value d. According to the total probability theorem, the hazard curve of the EDP can be calculated as:

$$\lambda_{EDP}(d) = \int P[EDP \geq d | S_a = x] \, |dH(x)| \tag{1}$$

in which the notation |·| means the absolute value of the derivative. $H(x)$ is the standard hazard curve, expressing the likelihood of future ground motion intensity exceeding a specified level x, in terms of spectral acceleration S_a. The hazard curve can be simply assumed to obey the power-law in the site of interest (Jalayer and Cornell 2003), and computed by:

$$H(x) = P[S_a \geq x] = k_0 x^{-k} \tag{2}$$

where k_0 and k are constant coefficients, which can be obtained through regression analysis between mean annual frequency and ground motion intensity of a specific location and soil conditions.

In equation 1, $P[EDP \geq d|S_a = x]$ is the likelihood that the EDP exceeds a specific value d given that the ground motion intensity S_a. Assuming a bivariate exponential relationship between the EDP and intensity measure S_a, the predicted EDP can be represented by:

$$EDP = a(S_a)^b \tag{3}$$

in which the parameters a and b can be obtained by conducting linear regression analysis of $lnEDP$ and lnS_a. Thus, with lognormality assumption and the $P[EDP \geq d|S_a = x]$ can be calculated as:

$$P[EDP \geq d|S_a = x] = 1 - \Phi\left(\frac{ln\,(d/ax^b)}{\beta_{EDP|S_a}}\right) \tag{4}$$

where Φ is the normal cumulative distribution function, and $\beta_{EDP|S_a}$ is the standard deviation of the logarithm of EDP conditioned on intensity S_a, implying the record-to-record uncertainty.

Seismic fragility analysis and seismic demand hazard analysis are both conducted with the common objective of evaluating the seismic performance of steel frames equipped with various damping systems. These risk-based evaluations commence with IDA using the 44 ground motions. In this study, the IDR and RIDR are considered as the engineering demand parameters, while the spectral acceleration corresponding to the fundamental period of the frame is selected as the intensity measure of the ground motions.

The seismic demand model refers to a mathematical representation of the relationship between the seismic intensity measure and the engineering demand parameters. Based on the results obtained from IDA and Equation (3), log-linear regression analyses are performed to establish the seismic demand models for IDR and RIDR for the SMA, SFD, and FD frames, as illustrated in Figure 5. The specific log-linear regression equations and corresponding coefficients of determination (i.e. R^2) are provided in the figure. A higher R-square value indicates a better fit of the regression model to the IDA data. It can be inferred that the regression model employed in this investigation exhibits superior predictive performance for IDR in comparison to RIDR.

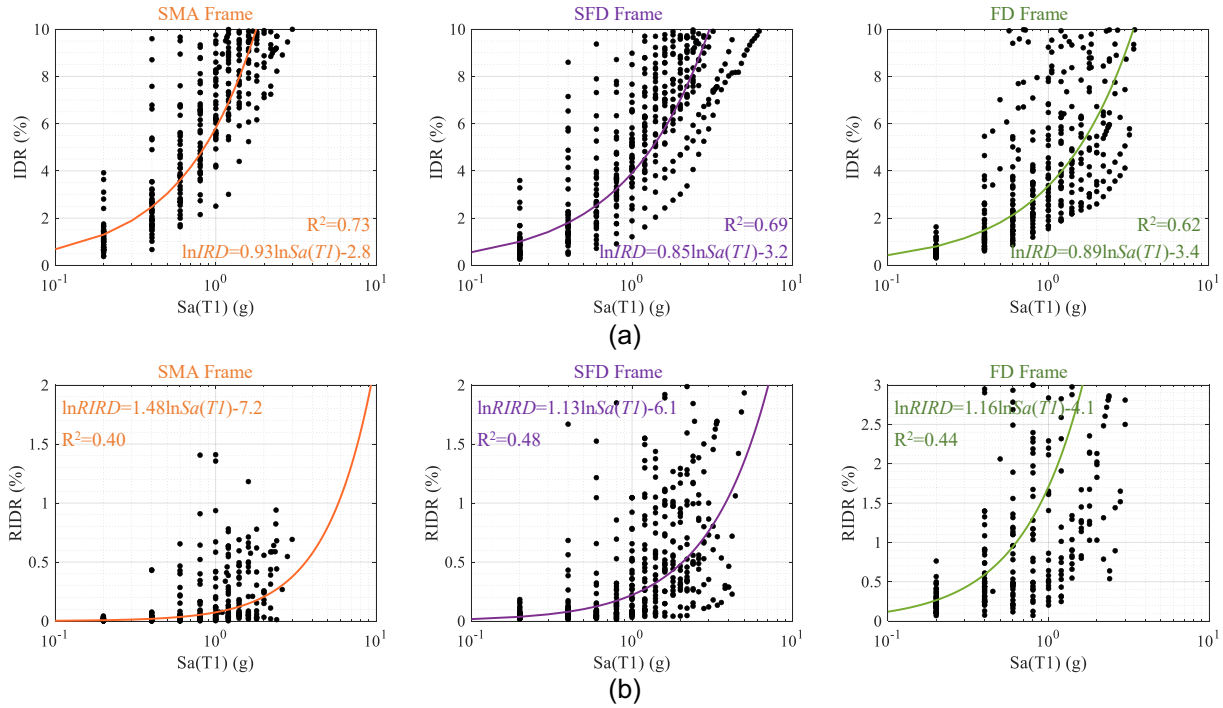

Figure 5. Log-linear regressions of (a) IDR versus Sa(T1) and (b) RIDR versus Sa(T1) for three case-study frames.

In order to conduct comprehensive comparisons among different damping systems, the IDR and RIDR are selected as performance indices to analyze the vulnerability of the three case-study frames. Three damage states (DS) are established to quantify the extent of damage for these frames. The specific damage states for seismic fragility analysis in this study are presented in Table 2. For IDR, the corresponding values for the three damage states are determined as 1.5%, 2.5%, and 3.75%, respectively, in accordance with the IDR limits specified by ASCE 7-16 under the FOE, DBE, and MCE hazard levels. Conversely, for RIDR, the corresponding values recommended by FEMA P58 are 0.2%, 0.5%, and 1.0%.

Table 2. Damage states for seismic fragility analysis

Performance Index	Damage State		
	DS1	DS2	DS3
IDR	1.5%	2.5%	3.75%
RIDR	0.2%	0.5%	1.0%

Figure 6(a) presents a comparison of IDR-based fragility curves at three different damage states for the SMA, SFD, and FD frames. It can be observed that, for the DS3 damage state, the S_a values corresponding to a 50% probability of exceedance are 1.87 g, 2.59 g, and 3.10 g for the SMA, SFD, and FD frames, respectively. Furthermore, the fragility curve for the SMA frame exhibits the steepest slope, followed by the SFD frame and the FD frame, indicating that the SMA frame is more susceptible to reaching this damage state at a lower level of ground motion intensity. This can be attributed to the lower energy dissipation capacity of the SMA damper. Frames equipped with damping systems that possess better energy dissipation capacity, such as the FD frame, are less prone to damage in terms of IDR. This pattern holds true for the DS2 and DS3 damage states as well. However, the trend is precisely opposite for the RIDR-based damage states. Figure 6(b) illustrates the RIDR-based fragility curves for DS1, DS2, and DS3 for the three case-study frames. The frame equipped with the SMA damper exhibits the least slope among the fragility curves and demonstrates the best performance in terms of RIDR at all three damage states. Particularly for the DS3 damage state, frames equipped with self-centering dampers (i.e., SFD and SMA damper) have an extremely low probability of RIDR exceeding 1%, indicating that the self-centering frames possess excellent reparability and resilience after experiencing a severe earthquake event. Based on the fragility analysis results using IDR and RIDR damage states, it can be concluded that the SFD offers an optimal balance between energy dissipation capacity and self-centering ability, resulting in structures with minimal transient response and residual response.

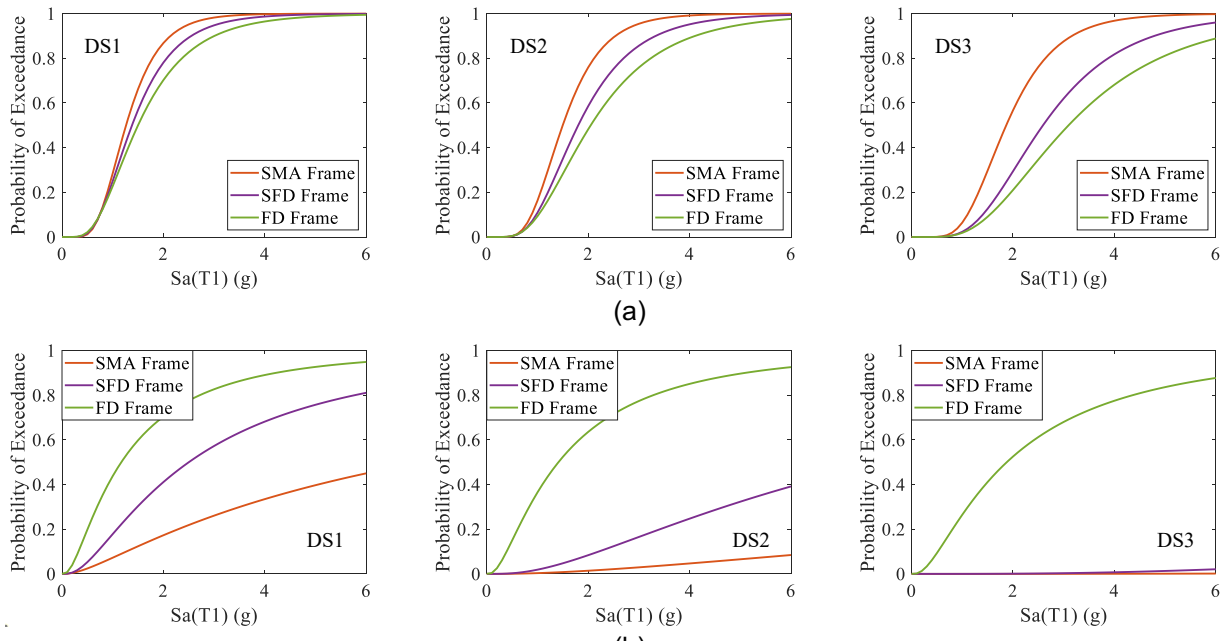

Figure 6. (a) IDR-based, and (b) RIDR-based fragility curves at various damage states for three case-study frames.

The hazard curve is a graphical representation of the probability of exceeding a specified ground motion intensity level (S_a) within a given time period. By conducting regression analysis based on the Mean Annual Frequency (MAF) and spectral acceleration intensity for the Design Basis Earthquake (DBE) and Maximum Considered Earthquake (MCE) hazard levels, the coefficients of Equation (2) can be determined. Figure 7 illustrates the hazard curves for the three case-study frames, corresponding to their respective fundamental periods. The hazard curves of the SMA frame and SFD frame exhibit significant overlap due to their comparable fundamental periods. Conversely, the frame with a relatively shorter fundamental period (i.e., the FD frame) demonstrates a higher mean annual frequency for the same S_a intensity level.

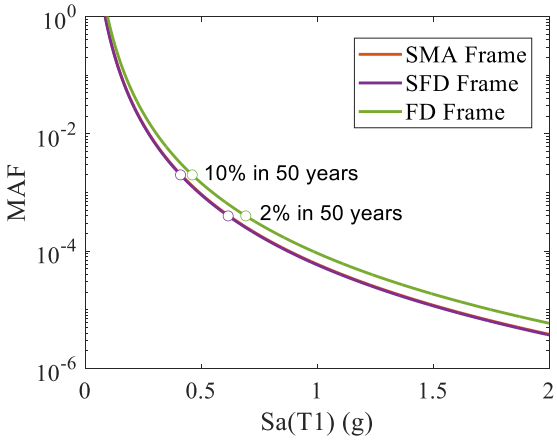

Figure 7. Hazards curves for three case-study frames.

By integrating the hazard curves and seismic demand models using Equation (1), the IDR and RIDR hazard curves for frames with different dampers can be calculated. These hazard curves quantify the likelihood of experiencing a certain level of structural response due to seismic events of varying intensities, allowing for the evaluation of frame performance with different damping systems. Figure 8 provides a comparison of the IDR and RIDR hazard curves for the three case-study frames. It can be observed that the Mean Annual Frequency (MAF) decreases as the IDR and RIDR increase. The IDR hazard curves of the three frames exhibit an intersection phenomenon. Specifically, the SMA frame shows a lower MAF under lower IDR demands. However, as the IDR demand increases and the energy dissipation capacity becomes critical, the FD frame outperforms the SMA frame, while the SFD frame demonstrates comparable performance to the FD frame. Regarding the RIDR hazard curve, it can be inferred that the performance of frames equipped with SMA or SFD dampers has considerably improved compared to the FD frame. There is also an intersection in the RIDR hazard curves of the SMA and SFD frames, which can be attributed to the slight residual deformation inherent in the SFD.

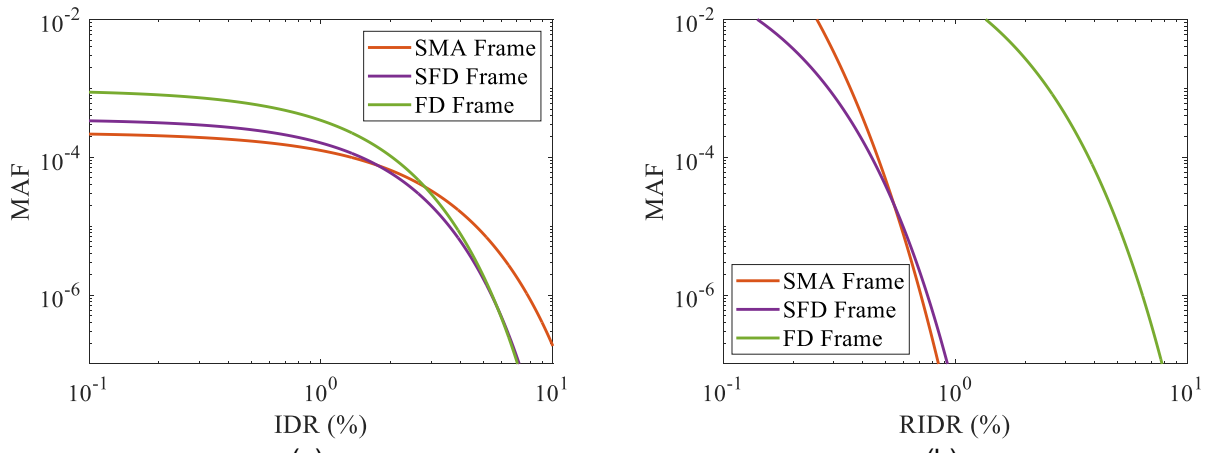

Figure 8. Comparison of the (a) IDR and (b) RIDR hazard curves for three case-study frames.

To facilitate a more comprehensive and rigorous quantitative comparison, the MAF values for the SMA, SFD, and FD frames are calculated at three different damage states, considering both IDR and RIDR responses. The computed MAF values for all three case-study frames are presented in Table 3. The obtained results reveal that the difference in MAF for IDR between the SMA and SFD frames at the DS1 damage state is negligible, with a difference of less than 10%. However, at the DS2 and DS3 damage states, the MAF values of the SFD frame are significantly lower compared to those of the SMA and FD frames, indicating superior performance for the frame equipped with hybrid Self-Centering Friction Dampers (SFDs). Regarding the MAF values for RIDR, the FD frame exhibits inferior performance compared to the other two frames due to the absence of a self-centering mechanism. Conversely, the MAF values of the SFD frame are lower than those of the SMA frame at the DS1 and DS2 damage states for RIDR. Although there is a slight increase in the MAF values for the SFD frame at the DS3 damage state, the probability of exceeding this damage state (i.e. 3.65×10^{-8}) can be considered infinitesimally small. Overall, within the range of IDR and RIDR of interest, the SFD frames exhibit superior seismic performance by leveraging the benefits of self-centering and energy dissipation abilities. This inherent characteristic of the hybrid SFD device places the SFD frame at a significant advantage over the other two case-study frames evaluated in this study.

Table 3. Mean annual frequency of specified damage states for case-study frames

Case-study Frame	IDR-based Damage State			RIDR-based Damage State		
	DS1 (1.5%)	DS2 (2.5%)	DS3 (3.75%)	DS1 (0.2%)	DS2 (0.5%)	DS3 (1.0%)
SMA Frame	9.03×10^{-5}	4.59×10^{-5}	1.91×10^{-5}	3.82×10^{-2}	4.84×10^{-5}	8.55×10^{-9}
SFD Frame	9.90×10^{-5}	3.43×10^{-5}	8.11×10^{-6}	3.74×10^{-3}	3.91×10^{-5}	3.65×10^{-8}
FD Frame	1.90×10^{-4}	5.51×10^{-5}	1.07×10^{-5}	1.38×10^{-1}	6.52×10^{-2}	2.11×10^{-2}

5 Conclusions

The seismic performance evaluation of a steel frame building, designed with hybrid self-centering devices that combine the recentering capability of SMA cables with the energy dissipation capacity of frictional devices, is conducted within a risk-based seismic demand analysis framework. This evaluation involves both seismic fragility analysis and seismic demand hazard analysis. A comparative assessment is then carried out by contrasting the results obtained from the building equipped with hybrid devices with those obtained from structures equipped with either frictional dampers or SMA devices. Based on the findings, the following conclusions can be drawn:

- The SFD, which integrates the mechanical characteristics of SMA cables and frictional devices, demonstrates the ability to recover approximately 90% of the imposed deformation. This showcases its exceptional self-centering capability and strong energy dissipation capacity, exhibiting minimal dependency on frequency.
- Under the DBE and MCE hazard levels, the SFD Frame exhibits a comparable RIDR response to the SMA Frame due to its excellent self-centering ability. Additionally, it demonstrates comparable IDR and AA responses to the FD Frame, owing to its contribution to energy dissipation capacity.
- Fragility analysis results indicate that the SFD effectively balances the advantages of self-centering capability and energy dissipation capacity. The steel frame equipped with SFDs exhibits a balanced seismic response across all three damage states in terms of IDR and RIDR responses.
- A comprehensive risk-based seismic hazard assessment is conducted by evaluating IDR hazard curves, RIDR hazard curves, and MAF at three damage states for all three case-study frames. Within the range of seismic demands of interest, the frame integrated with SFDs demonstrates superior seismic performance compared to the other frames. The hybrid SFD effectively harnesses the capacity for energy dissipation and self-centering, enhancing structural resilience and reducing vulnerability to seismic hazards.

6 References

Asfaw, A. M., Cao, L., Ozbulut, O. E., & Ricles, J. (2022). Development of a shape memory alloy-based friction damper and its experimental characterization considering rate and temperature effects. Engineering Structures, 273, 115101.

Erochko, J., Christopoulos, C., & Tremblay, R. (2015). Design, testing, and detailed component modeling of a high-capacity self-centering energy-dissipative brace. Journal of Structural Engineering, 141(8), 04014193.

Fang, C., Qiu, C., Wang, W., & Alam, M. S. (2023). Self-Centering Structures Against Earthquakes: A Critical Review. *Journal of Earthquake Engineering*, 1-36.

FEMA (2012). *Seismic performance assessment of buildings (FEMA P-58)*. Federal Emergency Management Agency.

Gupta, A., & Krawinkler., H. (1999). *Seismic demands for performance evaluation of steel moment resisting frame structures*. Technical report 132. The John A. Blume Earthquake Engineering Research Center, Department of Civil Engineering, Stanford University, Stanford, CA.

Harris, J.L., & Speicher, M.S. (2015). *Assessment of First Generation Performance-Based Seismic Design Methods for New Steel Buildings Volume 1: Special Moment Frames - NIST Technical Note 1863-1*. National Institute of Standards and Technology, Gaithersburg, MD.

Ibarra, L.F., Medina, R.A., & Krawinkler, H. (2005). Hysteretic models that incorporate strength and stiffness deterioration. *Earthquake Engineering & Structural Dynamics*, 34(12): 1489‐1511.

Jalayer, F., & Cornell., C.A. (2003). *A technical framework for probability-based demand and capacity factor design (DCFD) seismic formats, PEER Report 2003/08*. Pacific Earthquake Engineering Research Center, University of California, Berkeley.

Ozbulut, O. E., Hurlebaus, S., & DesRoches, R. (2011). Seismic response control using shape memory alloys: a review. *Journal of Intelligent Material Systems and Structures*, 22(14), 1531-1549.

Ping, Y., Fang, C., Shi, F., et al. (2022). Experimental and numerical studies on SMA-viscoelastic hybrid self-centering braces. *Smart materials and structures*, 31: 095048

Shi, F., Zhou, Y., Ozbulut, O. E., & Ren, F. (2022). Hysteretic response and failure behavior of an SMA cable-based self-centering brace. *Structural Control and Health Monitoring*, 29(1), e2847.

Shi. F., Lin. Z., Li. Q., et al. (2023) Design, manufacturing, and testing of a hybrid self-centering brace for seismic resilience of buildings. *Earthquake Engineering & Structural dynamics*, 52(5): 1381-1402.

Xiao, Y., Eberhard, M. O., Zhou, Y., Stanton, J. F., & Shen, J. (2022). Experimental investigation of a low‐prestressed self‐centering energy dissipative brace. Earthquake Engineering & Structural Dynamics, 51(6), 1457-1476.

Xu, L. H., Fan, X. W., & Li, Z. X. (2016). Development and experimental verification of a pre-pressed spring self-centering energy dissipation brace. Engineering Structures, 127, 49-61.

Zhong, C., & Christopoulos, C. (2022). Self-centering seismic-resistant structures: Historical overview and state-of-the-art. *Earthquake spectra*, 38(2), 1321-1356.